MECHANISM FOR DETECTING NAPL IN GROUNDWATER WITH RESISTIVITY

By

VALINA SEFA

Bachelor of Science in Environmental Science

East Central University

Ada, OK

2012

Submitted to the Faculty of the
Graduate College of the
Oklahoma State University
in partial fulfillment of
the requirements for
the Degree of
MASTER OF SCIENCE
July, 2015

MECHANISM FOR DETECTING NAPL IN

GROUNDWATER WITH RESISTIVITY

Thesis Approved:

Dr. Todd Halihan

Thesis Adviser

Dr. Estella Atekwana

Dr. Tyson Ochsner

ACKNOWLEDGEMENTS

This research would have not been possible without the help and the support of many people. I want to offer thanks to my advisor, Dr. Todd Halihan, for his guidance, patience and support. His cheerful attitude on daily basis made going to his office for guidance a joyful experience. I want to thank Colorado State University with special thanks to Dr. Tom Sale, Dr. Julio Zimbron and Alison Hawkins for allowing us to use their facilities and their sand tank and for helping conduct the experiment. Thanks to Chevron and Mark Lyverse for providing the financial support for this research. A special thank you goes to Robert Reynolds for processing the ERI data. Also, thanks to my committee members, Dr. Estella Atekwana and Dr. Tyson Ochsner, for their guidance and support.

I would like to extend my gratitude to Dr. Lowell Caneday for taking me as his research assistant. He supported me emotionally and financially throughout this process. Also, I want to give a big thank you to all the faculty, staff and fellow students at Oklahoma State University for their advice and technical support.

Last but not least, thank you to my friends and family for taking this journey with me. I especially want to thank my brother, Fanar Sefa, for listening to me ramble about my work and helping me with edits.

Name: Valina Sefa

Date of Degree: JULY, 2015

Title of Study: Mechanism for detecting NAPL in groundwater with resistivity

Major Field: Environmental Science

Abstract:

The detection of low concentrations of non-aqueous phase liquids (NAPLs) in freshwater environments by electrical resistivity imaging (ERI) has been clearly demonstrated in field conditions, but the mechanism that generates the resistive signature is poorly understood. An electrical blocking mechanism for detecting low concentrations of non-aqueous phase liquids with electrical resistivity is tested by first developing a theoretical basis for the mechanism, testing the mechanism in a two-dimensional sand tank with electrical resistivity imaging (ERI), and finally performing forward modeling of the laboratory experiment.

The NAPL blocking theory assumes that at low bulk saturations, NAPL can block pore throats and generate an electrically resistive signal. The sand tank experiment utilized a photographic technique to quantify petroleum saturation in conjunction with ERI to determine if ERI can detect and quantify NAPL across the water table. This experiment demonstrates that electrical methods can detect NAPL of sufficient thickness with the relationship indicating that the bulk volume of NAPL is not the controlling variable for the amount of resistivity signal generated. The signal is due to a layer with high resistivity blocking current flow through the impacted zone. Thicknesses of impacted zones of 3.3 cm and higher were detected in this tank experiment causing a change in resistivity of 2% and greater. The maximum change in resistivity from the tank experiment was an increase of 37%. Forward models of the experiment confirm the blocking mechanism for the tank experiment.

TABLE OF CONTENTS

LIST OF FIGURES

Figure Page

CHAPTER I

INTRODUCTION

1.1 The NAPL problem

Non-aqueous contaminants (those that do not dissolve easily into water) are categorized in two groups: light non-aqueous phase liquids (LNAPLs) and dense non-aqueous phase liquids (DNAPLs). Many cases of NAPL releases are identified at the time of the spill but many others are not discovered until after products appear in surface water or groundwater wells. Depending on the amount released, NAPLs can either be trapped in the vadose zone by capillary forces or can migrate downwards through the vadose zone to the water table because of gravity. For LNAPLs, although there are exceptions, in many cases once the hydrocarbons have reach the water table, the pressure gradients causes them to spread laterally on top of the water table. Hydrological studies have shown that LNAPLs do not dissipate uniformly in homogeneous manner, but they move through the unsaturated zone in discontinuous accumulations creating NAPL "blobs" or pools (Newell, 1995). DNAPLs can form more complex distributions as they are heavier than water and can more easily migrate below the water table (Brewster et al., 1995).

In 2013, the United States consumed over 130 billion gallons of gasoline (U.S Energy Information Administration, 2014). This high demand for gasoline has led to improvements of the management practices used for production, transportation, refining and storage of the petroleum products. These practices have reduced the number of petroleum releases, but unfortunately have not eliminated petroleum leaks into the subsurface. Petroleum products are accidentally released into the subsurface through spills, leaking pipelines, leaking underground or above ground storage tanks, and through other means. These petroleum products when released in significant quantities threaten public health and safety. Such releases contaminate ground water, diminish air quality,

increase the risk of fire and explosion hazards, and waste nonrenewable resources (U.S. EPA, 2014). A release also negatively impacts ecosystems (U.S. EPA, 2014).

Similar to the situation with LNAPL`s the widespread production, transportation, use and disposal of DNAPL`s is generating many DNAPL contaminated sites. DNAPL`s present a high risk of groundwater contamination because of their toxicity, limited solubility, and significant migration potential (soil gas, groundwater, and separate phase liquids). One of the most common groundwater contaminants found in groundwater supplies and waste disposal sites are DNAPL`s, such as chlorinated solvents (US. EPA, 2014).

Traditionally, local and federal governmental regulations mandate that all contaminated sites are characterized to restore and create a safe environment for those who live around these sites. Typically, characterization includes determining the magnitude and extent of the spill, the release`s hydrological characteristics, and the potential pathways that the release could follow. This process of characterizing the released NAPL and its subsequent migration has been challenging for scientists and engineers involved in soil cleanup and remediation.

Two traditional detection and monitoring strategies are primarily used for site characterization. The first strategy is to utilize point sampling using monitoring wells or multilevel piezometers. The second, involves making indirect subsurface measurements using surface or borehole geophysical techniques (Halihan et al., 2005). Cost is the primary disadvantage of the point sampling technique due to the expenses associated with drilling, sampling and interpretation time. This technique can also miss contaminants in the areas where well data are not available. A solution to these issues is to utilize electrical geophysical data to obtain a more complete data coverage of the site within a shorter period of time. Electrical Resistivity Imaging (ERI) is used to delineate the boundaries of an impacted area and is a more efficient and cost effective method than drilling numerous monitoring wells (Benson and Mustoe, 1998; Halihan et al., 2005).

Previous studies have demonstrated that ERI can be used in fresh water environment to detect petroleum at parts-per-million concentrations (Halihan et al., 2005). However, quantifying the results is difficult because of a lack of understanding of

the mechanism that controls the electrical resistivity difference generated from the petroleum products in the pore space.

1.2 Mechanisms

In the petroleum industry, apparent resistivity measurements were used to investigate the distribution of petroleum early in the twentieth century. In 1929, four electrode arrays were adapted in well logging for petroleum exploration (Rust, 1938). In 1942, Gus Archie saw a simple relationship between resistivity of sand when all the pores are filled with water (R_0), resistivity of the pore fluid (R_W), and the formation resistivity factor (F) (Archie, 1942). This relationship is shown below:

$$R_o = F R_w$$

Additionally, Archie investigated the relationship between the resistivity of sand (R) and the percentage of the pores filled with water (S) which is now known as Archie's law:

$$R = \phi^{-m} S_w^{-n} R_w \text{ or } \rho = \phi^{-m} S_w^{-n} \rho_w.$$

where ρ [ohm-m] is the bulk resistivity of the porous media , ϕ is the porosity, m is the cementation factor (usually ranges between 1.8 and 2), n is the saturation exponent (usually close to 2), S_w is water saturation or the percent of pores filled with water and ρ_w [ohm-m] is the resistivity of the pore fluid.

In the early 1950`s the geometric factor, $a$, was utilized to account for the effects of tortuosity, transforming Archie`s equation to:

$$\rho = a\ \phi^{-m} S_w^{-n} \rho_w$$

Based on the pore- network models, NAPL contaminated sites are not usually water- wet. During oil migration the oil invades the pore spaces by primary drainage process. When the oil contacts the solids surface, the surface –active components of oil attach to the surface changing its wettability. In three phase flow models (water, oil and gas) oil forms a layer sandwiched between water and gas in water- wet and mixed wet pores (Blunt, 2001). This water displacement in NAPL contaminated sites causes the water saturation (S_w) and the resistivity of the pore fluid (ρ_w) to change, which influences the strength and the value of the geophysical signal generated when performing geophysical measurements (Atekwana et al., 2000).

Studies have shown that electrical methods are successful in detecting immiscible contaminants in subsurface because of the large difference in electrical properties between the immiscible contaminants and the water (Endres and Redman, 1996). However, resistive LNAPL has been detected in fresh water environments at very low concentrations (Halihan, et, al 2005). And there is no existing theory to explain the mechanism behind this detection at parts per million concentrations.

1.3 Hypothesis

The goal of this research was to determine the mechanism for detecting small quantities of non-aqueous phase liquids (NAPL) in subsurface environments with electrical resistivity. The hypothesis is that small quantities of NAPL create a barrier with sufficient NAPL saturations that decrease the current flow resulting in an increase of bulk resistivity of the media. This hypothesis can be tested by 1) using a theoretical model calculating the concentration / saturation required to form a resistive barrier, 2) laboratory tank testing of the mechanism to evaluate the theoretical work and compare against known field experiments and, 3) forward modeling of resistivity to determine if a sufficient signal is available.

CHAPTER II

PREVIOUS WORK

Previous literature relevant to this study includes research on NAPL migration and monitoring using a sand tank as well as electrical resistivity imaging. This chapter includes 1) Electrical resistivity mechanisms for signal generation, 2) Geophysical monitoring of simple NAPL migration, and 3) NAPL tank experiments (optical and electrical NAPL monitoring).

2.1 Electrical Resistivity Imaging (ERI)

Geophysical prospecting with electrical methods began in the 1830`s when Robert W. Fox measured the natural current of sulfide ore deposits at Cornwall, England (Burger et al., 2006). The aim of electrical surveys is commonly to measure the resistivity distribution in the subsurface in order to obtain useful information about the distribution of materials or processes in the subsurface (Loke, 2000; Smith and Sjogren, 2006).

Resistance is the tendency of a material to resist the flow of current. More precisely, the resistance (**R**) is defined by Ohm`s Law as (Telford et al., 1990):

$$R = V/I \ [Ohm]$$

where **V** [volts] is the potential difference, or voltage drop, and **I** [amps] is the current that is passing through the material. The resistance of a material is directly related to the length L [m], and inversely related to its cross-sectional area, **A** [m^2], by expression:

$$R = \rho \ (L/A)$$

where ρ [Ohm –m], is a constant of proportionality called resistivity (Telford et al., 1990). In earth materials, the most common type of conduction is electrolytic, because the pore space fluids act as conductors while grains provide little conductivity (Reynolds,

2011). The resistivity of the subsurface is measured in [Ohm–m] and is a function of porosity, saturation, resistivity of the pore fluids and the solid phase, and the material texture (Loke, 2000; Nyquist et al., 2008; Smith and Sjogren, 2006).

Electrical Resistivity Imaging (ERI) is a geophysical technique that measures the resistivity distribution of the subsurface using an array of electrodes instead of only four. Electrode arrangement is critical because it can affect the depth of investigation, sensitivity, resolution, and the incorporation of noise into each apparent resistivity measurement (Smith and Sjogren, 2006). Resistivity measurements are accomplished by injecting current into the ground through two electrodes (commonly referred to as *A* and *B*) and measuring the voltage difference at two potential electrodes (commonly referred to as *M* and *N*). The "apparent" resistivity (ρ_a) is a function of the current (I), voltage (V) values and the geometric factor (k). The geometric factor depends on the four electrode arrangement. In the case of evenly space electrodes, the apparent resistivity is calculated by the following expression:

$$\rho_a = k\,(\Delta V/I)$$

The "apparent" resistivity is not the true resistivity of the subsurface. To determine the true resistivity values of the subsurface, apparent resistivity datasets must undergo data inversion. Through data inversion processing, ERI methods can produce two and three dimensional subsurface images, providing a better understanding of subsurface materials composition (Bentley and Gharibi, 2004; Smith and Sjogren, 2006). Although resistivity surveys were utilized for several decades, it was not until the 1990's that data acquisition technology and the inversion processing software made it possible to produce accurate 2D and 3D electrical images of the subsurface. Modern ERI imaging technology is described as a combination of traditional electrical probing introduced by Schlumberger brothers in the 1930s and cutting-edge tomography data inversion methods (Daily et al., 2004).

2.2 Geophysical Monitoring of Simple NAPL Migration

Geophysical techniques, such as electromagnetic (GPR) and electrical resistivity (ERI), have been used numerous times to delineate and monitor NAPL contamination

plumes. Electrical methods have a high success rate on detecting NAPL in the subsurface because of the different electrical properties between the host formation and the invading fluids (NAPL). Sites contaminated with fresh LNAPL generally generate a high resistive signal (Benson et al., 1997; Delaney et al., 2001; DeRyck et al., 1993; Yang et al., 2007). Many studies support the theory that NAPLs can be detected because the zone with NAPL has higher resistivity, and lower permittivity, than the uncontaminated zone. This conclusion is supported by many laboratory experiments that used fresh hydrocarbon as a contaminant (Daniels et al., 1992; DeRyck et al., 1993; Endres and Redman, 1996; Monier-Williams, 1995).

Conductive resistivity values can also exist over a NAPL impacted site. A study done over a fifty year old hydrocarbon contaminated site showed conductive values over the LNAPL plume relative to the surrounding area (Atekwana et al. 2000). The authors concluded that the electric signal changed from resistive to conductive as a result of LNAPL biodegradation. During biodegradation, biofilms can grow over LNAPL materials acting as electrical conductors also biological processes that convert LNAPL to carbonic and organic acid add ions to solution, each enhancing the conductance of the geophysical signal (Atekwana et al., 2000).

Geophysical techniques were also used to evaluate DNAPL contaminated sites (Daniels et al., 1992; Schneider and Greenhouse, 1992). Electrical resistivity tomography (ERT) (ERI with electrodes placed into the subsurface) was used in laboratory column as well as in field- scaled in suite bioremediation site to monitor DNAPL migration and observe its electrical signal. In both settings DNAPL generated resistive anomalies and ERT was able to delineate the pathways of the DNAPL migration (Chambers et al., 2004; Chambers et al., 2010).

Studies have shown a good correlation between the data retrieved from monitoring wells and the electrical resistivity data when delineating NAPL plume boundaries (Benson et al., 1997). Conversely, in a study done in a previously contaminated site, ERI detected “blobs” of hydrocarbon both inside and outside of the remediated area. Hydrocarbons were also detected between “clean” monitoring wells (Halihan et al., 2005).

2.3 NAPL Tank Experiments

Optically Quantified NAPL

Two-dimensional sand tanks have been utilized in many experiments to investigate and to monitor the migration of the NAPL in porous media. Researchers have experimented with different types of sand (30/50 silica, coarse grain, fine grain, etc.) and various techniques (multispectral image analysis, resistivity probes, tensiometers etc.). Nonetheless, the final results and conclusions were analogous. In these experiments the plume migration seemed to follow the same movement. The initial pattern of the LNAPL plumes formed a sharp, rounded front moving downward through the unsaturated zone at high LNAPL saturation, compressing the capillary fringe above the water table, and then migrating laterally forming a pancake shaped lens (Neumann et al., 2000; Van Geel and Sykes, 1994).

Dense non-aqueous phase liquids (DNAPL) migration processes have also been investigated in laboratory-scale sand tanks that were used to simulate groundwater and unconfined aquifer contaminant transport (Hofstee et al., 1998; Kamon et al., 2004; Oostrom et al., 1999). In an experiment utilizing DNAPL in form of perchloroethylene (PCE) infiltrated through different layers of sand, it was found that PCE accumulated in the water-unsaturated fine-grained layer and moved both vertically and horizontally (Hofstee et al., 1998). However, experimenting in a tank filled with Toyoura sand (clean homogeneous sand), DNAPL prefers bilateral migration over vertical migration, forming an elliptical spread at the spillage point when lateral groundwater flow is not present (Kamon et al., 2004). Another study also shows that in the absence of the lateral groundwater flow and DNAPL migration, the resulting micro-emulsion that forms when the surfactant solubilizes, tends to migrate downward due to its density contrast with the surrounding water (Kostarelos et al., 1998).

Florescent dyes and UV lights were employed to a sand tank experiment to determine LNAPL flow rates through simulated wells and adjacent formations (Sale et al., 2007). Furthermore, fluorescent dyes and UV lights were utilized to research the diffusion of contaminant into and out of low permeability zones (Chapman et al., 2012). These experiments utilized clean white electrically resistive sand to provide a good visual contrast for quantifying NAPL.

The sand tank used in this experiment was previously utilized in Colorado State University tank experiments (Hawkins, 2013). The experiment conducted was done to explore governing processes of NAPL releases at groundwater surface water interfaces (GSIs). In her experiment Hawkins employed fluorescent dyes (BSL 715, a.k.a. StayBrite) and UV light (black lights) to enhance the visualization of NAPL behavior in the tank. Utilizing Adobe® Photoshop ® 7.0 (Adobe®, San Jose, CA) and MATLAB® (MathWorks®, Natick, MA) Hawkins was able to produce saturation curves from the digitally enhanced images taken during the experiment. The technique of converting digital images to saturation curves was initially created by Dr. Julio Zimbron (Hawkins, 2013).

Electrical Tank Experiments

Electrical resistivity evaluations of geologic processes via tank experiments have been common since the 1960s. Apparao et al. (1969) used a tank to see the resistivity profile over simulated veins and sheets. The authors used two types of electrode configurations, the Wenner arrangement and the lateral log. A mixture of graphite and cement was utilized to model the veins and provided a strong enough model to collect usable data. Before Apparao's experiment, it was recommended that point source approximations should be evaluated when conducting tank experiments. Field experiments are much larger than tank experiment and it is important to determine if ERI field experiments can be scaled down to tank dimensions (Cook and Van Nostrand, 1954).

Resistivity tank experiments were used to investigate different prospects. In an experiment where the resolution of resistivity imaging was investigated the authors concluded that the Wenner configuration was the most efficient means to detect thick dykes; however, the Schlumberger configuration had a better resolution and configuration for thin dykes (Singh et al., 1971). Another experiment used a resistivity tank to conduct ground electrode resistance measurements in non-homogenous soils. From this experiment the authors concluded that earth resistance measurements are very sensitive in homogenous soils. As a result one must take into consideration several parameters including the electrode spacing, the resistivity variation, the ground electrode

dimension and shape when conducting ERI measurements (Dawalibi and Mukhedkar, 1974).

Resistivity tank experiments were also utilized to investigate solute transport processes. A 3D ERT experiment concluded that cross-hole electrical imaging and 3D ERT are powerful tools in quantifying solute transport processes (Slater et al., 2002). A 2D electrical resistivity time lapse tank experiment modeled the leakage of petroleum products from underground pipelines. It was concluded that high resistivity values are directly related to hydrocarbon accumulation, and the decrease in resistivity is a result of hydrocarbon draining into the deeper levels of the tank (Adepelumi et al., 2006). ERT and an agitated tank equipped with a top entering axial-flow impeller were used to investigate the solid-liquid mixing. The degree of homogeneity was quantified by correlating the ERT measurements and solid concentration profiles (Hosseini et al., 2010).

CHAPTER III

METHODS

A sand tank experiment was conducted to determine the petroleum distribution mechanism that governs the strength of the electrical resistivity signal generated from NAPLs saturations. The methods described include: 1) theory for a NAPL resistive barrier mechanism, 2) Tank set up - optical, 3) Tank set up - electrical, and 4) Forward resistivity models.

3.1 NAPL Resistive Barrier Mechanism

To develop a theoretical basis to understand the phenomenon of detecting NAPL with electrical methods at low concentrations in porous media, the conceptual idea of spherical uniformly packed porous media was used to evaluate a NAPL resistive barrier theory. In this theory, the NAPL provides a thin electrically resistive layer that can block the flow of current via a more resistive separate phase fluid than the water in the pore spaces. The spheres represent the solid grains of the media with a high resistivity (ρ_s), and the space between them represents the volume filled with liquid with a resistivity of (ρ_w). The NAPL with a higher resistivity than the water (ρ_n) (NAPL) blocks a small amount of the pore space in a layer (Figure 1). The volume of NAPL can be calculated by subtracting the volume of the solid grains from the total volume of cube times the NAPL thickness. This geometry provides the minimum amount of NAPL required to generate a detectable signal in the media. Actual NAPL distributions would require a higher thickness. An estimate is made for the geometry of a thin NAPL film and the resulting volume of NAPL in the media.

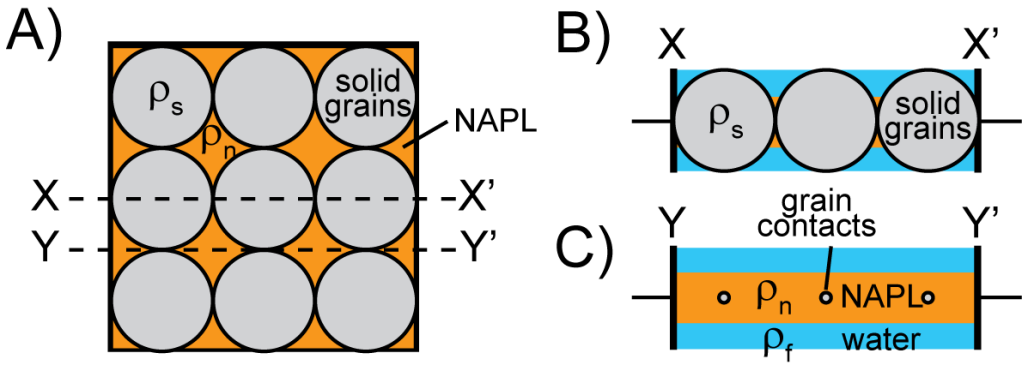

Figure 1. Signal generation theory for NAPL based on blocking electrical current: a) Plan view of NAPL in pore space b) Cross sectional view where particles block electrical current c) Cross sectional view where NAPL blocks electrical current and provide a resistive barrier detection mechanism.

3.2 Tank setup – optical

A two-dimensional sand tank constructed by Colorado State University was utilized for this experimental research. The dimensions of the tank were 180 cm (horizontal length) by 38.5 cm (height) by 5.3 cm (width) (Figure 2). The front and the back of the tank were made of 1.27 cm thick glass. The sides and the bottom of the tank as well as the frame were constructed of aluminum with glass placed on the sides to make a non-conductive glass interior. The tank was supported on a metal frame table that had a non-conductive table top.

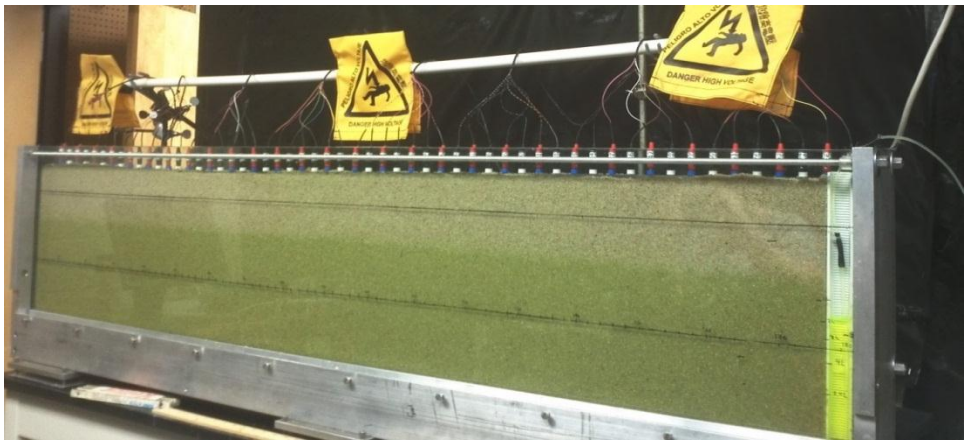

Figure 2. Photograph of the sand tank including resistivity electrodes.

The front of the tank was marked with a black line in centimeters from left to right. The right end of the tank had a permeable screen. The screen was constructed from round hole perforated stainless steel sheets (McMaster- Carr, Atlanta, GA) bent to 2.5 cm wide by 38.5 cm long by 5.3 cm deep. The screen was used to allow flow of water but prevented sand grains from entering Fluorinated Ethylene Propylene (FEP) 1/8" tubing (United States Plastic Corp, Lima, OH). The FEP tubing was used to alter water table levels to simulate NAPL smearing or tidal conditions. The tank was filled to a height of 35.5 cm with sand acquired from Colorado Silica Sand (Colorado Springs, CO) which had a porosity of 41%. The sand was washed prior to use to reduce fines, but was not sieved to maintain some minor amount of electrical conductivity to the media.

Water was introduced on the right hand side of the tank at a rate of 25 ml/hr until the water level reached 28 cm. The water had a fluid conductivity of 0.78 millisiemens/cm. A multichannel peristaltic pump connected to a Microsoft Windows computer was used to control the water levels during the experiment. The automated water level changes were completed using the LabView 8 computer program from National Instruments, Austin, TX. The NAPL was introduced on the left hand side of the tank using a compact multichannel peristaltic pump (REGLO model, ISMATEC, Glattburgg, Switzerland) at a rate of 1.9 ml/hr. An 18 gauge 1 ½ inch syringe needle (VWR, Radnor,PA) attachment at the end of FEP tubing allowed for NAPL to enter the tank at a precise location one centimeter above the top surface of the sand.

To enhance visualization of NAPL behavior in the sand tank, fluorescent dyes and UV lights (black lights) were employed. The NAPL used for this research was diesel.

Diesel has low solubility in water, low volatility, and a positive spreading coefficient. Its fluid density was measured and determined to be 0.85 g/cm^3. The diesel was then dyed with StayBrite (Brite Solutions Inc., Hollywood, FL) fluorescent dye at a concentration of 0.1% on a weight basis. The sand tank was filled with tap water and degassed by submitting it to 81.3 KPa vacuum for 3 hours. The water was then dyed with Fluorescein (Science Lab, Houston, TX) at a concentration of 0.25 % on a weight basis.

Two different types of lights were employed during this experiment. Two, 120 cm long, 40 W, T12 black lights were used to excite the fluorescent dyes and two portable, 10 W compacted florescent single – bulb lights were used to complement the black lights and allow the camera to capture non -fluorescent elements on the tank. Two digital single-lens reflex cameras where used to take pictures during this experiment. A Canon Rebel T21 was placed 150 cm away from the front-center of the tank. The second camera, a Canon Rebel XS1, was 120 cm away from the left half side of the tank and took pictures along the first 45 cm width of the tank. Both cameras were controlled by a Microsoft Windows computer using EOS Utility software.

To calculate the NAPL saturation curve and diesel mass, the digital images were cropped to smaller pieces called "element volumes" which were equal to the size of the ERI model pixel width. There were six "element volumes" identified in the original picture. The "element volumes" were cropped length wise at 10, 20, 30, 40 and 50 cm markers and one additional element was cropped at the location of the edge of the plume as it migrated. The dimensions of the element were 1.6 cm (horizontal length) by 20 cm (vertical height) (Figure 5d). To crop the element precisely at the dimensions listed above, a black line marked on the front of tank was used for scale. The element dimensions of 1.6 cm x 20 cm translated to approximately 113 pixels by 1465 photo pixels, respectively. It is imperative to note that digital photos between the two cameras had different resolutions, thus adjustments in the number of pixels were made to accommodate for differences.

Utilizing Adobe® Photoshop ® 7.0 and MATLAB®, the photos taken during the experiment were converted to binary pictures; enabling generation of NAPL saturation curves. The first step to creating an NAPL saturation curve is adjusting the color balance of the digital photo using Adobe® Photoshop ® 7.0. The color balance adjustment is

used to enhance the NAPL area in the photo and darken the remaining areas. The second step was utilizing a MATLAB® program, created by Dr. Julio Zimbron, to transform the digital photos to binary pictures and transform them to NAPL saturation curves. Binary pictures show the florescent NAPL converted to white and all other portions of the picture to black. Adjusting the luminescence level on the MATLAB® program created a better differentiation between the NAPL and other parts of the picture. Once the binary pictures were generated, the MATLAB® program averaged the NAPL saturation for every two rows of pixels and generated a NAPL saturation curve.

The total diesel mass in the tank [M] was calculated using the flow rate that the diesel was introduced into the tank, 1.9 [ml/hr], and the time when the digital image was taken. Additionally, the diesel mass for the "element volume" was calculated. This was achieved using the saturation data generated with MatLab and the volume of the "element volume". When all the masses of the "element volumes" were added together the total did not equal the total diesel mass in the tank due to the variation due to the depth of tank in the third dimension [M] and the pore distribution of the media. As a result a correction factor was introduced.

The correction factor was calculated using the following steps: 1) the area saturated with diesel was calculated, 2) the calculated area then was integrated vertically, 3) the diesel density and sand porosity were multiplied by the volume of the element, which yielding the calculated diesel mass [M_c], and 4) the total diesel mass [M] in the tank from the pumping rate over time was plotted against the calculated diesel mass from the photographic technique [M_c].

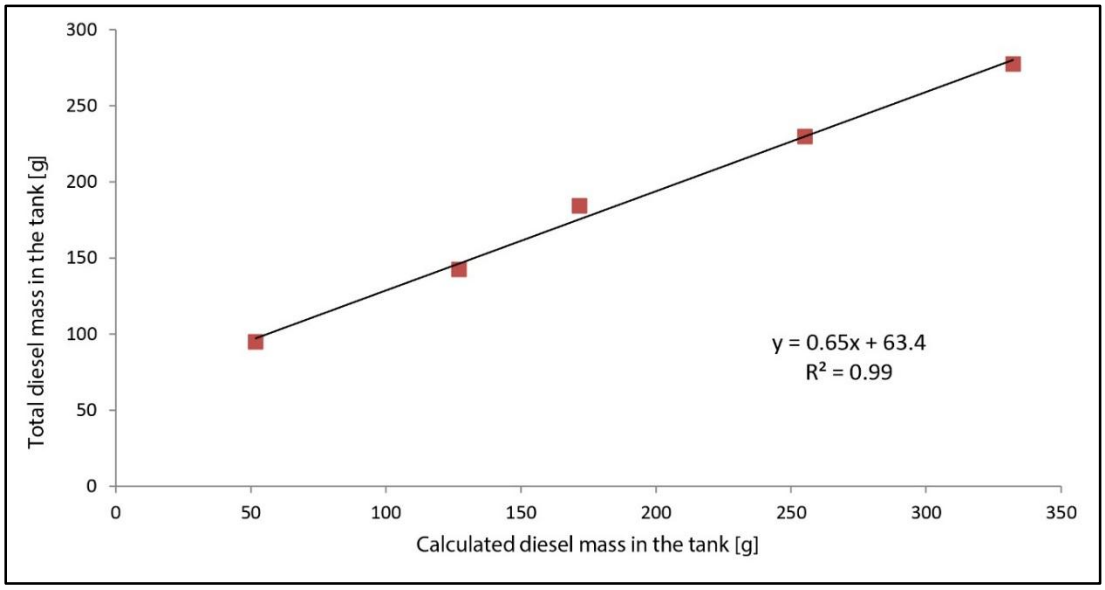

Figure 3. The correlation between the total diesel mass and calculated diesel mass in the tank.

These two variables had a strong linear correlation of $R^2 = 0.99$ (Figure 3). The correction was done by taking the calculated diesel mass of the element volume [Mc] and calculating the corrected visual mass**.** The error for the corrected visual mass values in the tank was within five percent of the actual mass values in the tank determined from the pumping rate.

3.3 Tank setup – electrical

The electric resistivity data during this experiment were collected using fifty-six electrodes connected to an AGI SuperSting R8 multichannel resistivity instrument (Figure 4). The electrodes were placed in two Poly (methyl methacrylate) (a.k.a Plexiglas) bars located on top of the sand in order to create uniform electrode spacing between all electrodes and allow them to penetrate the sand at the same depth. Each bar had twenty eight openings 3.175 cm apart (electrode spacing) creating an ERI line 174.6 cm long. Conductive medical gel (Signagel electrode gel, Parker Laboratories, Inc.) was used to create an improved, stable electrical connection between the dry resistive tank sand and the electrodes by coating the electrodes with gel prior to insertion into the top of

the tank. The setup was then covered to limit evaporation from the electrodes and the surface of the tank sand.

A standard dipole-dipole array and inversion with AGI Earth Imager 2D inversion and modeling software (AGI, Austin, TX) was utilized for the experiment. An Oklahoma State University Halihan / Fenstemaker ERI method of acquisition and inversion (Halihan/Fenstemaker method, OSU, 2004) was also utilized to acquire and process the data provide methods parallel to those utilized for equivalent field research (Halihan, 2005).

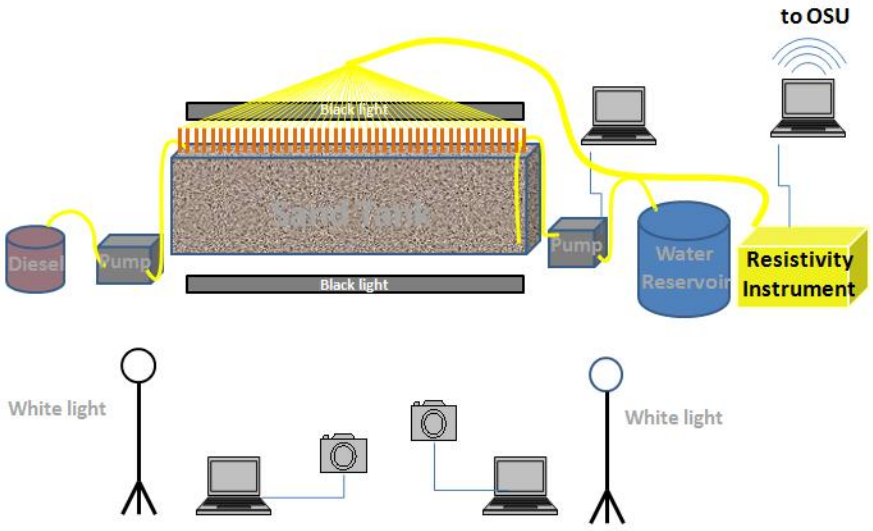

Figure 4. Schematic diagram of the experimental set-up.

3.4 Data acquisition

The experiment was carried out for seventeen days from September 19 – October 5, 2012. The stimulated diesel spill started on the second day of the experiment and continued for 338 hours, or a total of 14 days. The total amount of diesel spilled in the tank was 642 ml. In the final two days of the experiment, water table elevations were fluctuated to evaluate smearing (or tidal effects). The smearing caused the diesel mass to distribute more widely through the media to evaluate electrical barrier versus bulk volume signal generation mechanisms.

At the beginning of the experiment, electrical resistivity imaging data and digital photos were collected daily. During the smearing phase, the ERI data and the digital

photos were collected approximately every 6 hours. The data collected during the first day of the experiment were used as a reference background ERI data set. Moreover, the digital photos and the ERI data collected during days *2, 3, 4, 5, and 6* before tidal changes and days *13.8, 14.0, 14.3, 14.5, 14.8* during tidal changes were further processed and analyzed.

3.5 Resistivity forward modeling

Two sets of resistivity forward models were generated to compliment the experimental scenarios. These models were all three layer models where the first layer represented the vadose zone, ρ1 (1100 ohm-m), with a thickness of 10 cm, the second layer was the NAPL saturated media with a thickness ranging from 1.5 to 6 cm, ρ2 (2000 ohm-m), and the third layer reflected the water saturated zone, ρ3 (1000 ohm- m), with a thickness of 24 cm. Models were generated using both the standard approach and the Halihan / Fenstemaker method.

The first set of models were simple theoretical forward models that evaluated a three layer model where the middle layer simulated an NAPL saturated zone moving across the water table with a uniform thickness. For these models, the resistive layer, "the plume", started at 10 cm long and increased by 10 cm all the way to across the tank. For these simple theoretical forward models with one resistive layer going across the tank, additional stimulations were done to evaluate the strength of the NAPL signal in more conductive media. For this model the background resistivity was reduced in both the upper vadose layer and the lower phreatic layer to simulate the NAPL electrical signature in more conductive media.

The second set of forward models approximating the thicknesses and length of the plume from the tank experiment. The thicknesses and the lengths of the plume simulated the tank optical NAPL distribution data from 2, 4 and 6 days of the experiment.

CHAPTER IV

RESULTS

4.1 NAPL resistive barrier mechanism

The proposed mechanism suggested that the generation of detectable resistivity values in porous media was due to NAPL acting as an electrical barrier. In this case NAPL was blocking the pore throats over a sufficient area, creating a resistive layer. The plain view image shows how NAPL occupies the pore space and the percentage of the image filled with solid grains and the percentage filled with NAPL (Figure 1a). In the cross sectional view through the grains, the layer is primarily filled with solid grains and some NAPL (Figure 1b). In this cross section, the bulk NAPL concentrations are small, yet have a significant impact on the flow of electrical current as together with the solid grains block the electric current. The cross sectional view through the pore throats illustrates a case in which grains comprises a small portion of the NAPL layer space (Figure 1c). In this cross section the saturation of NAPL is high and acts as an insulating layer. This electrically resistive layer blocks the electrical signal and is the hypothesized source of the high resistivity signal generated in fresh water environments.

NAPL concentrations found with this structure can be calculated mathematically by determining the volume of pores that are occupied. By assuming a 1000 cm^3 volume filled with solid grains with 1 mm diameter, one can calculate the fluid volume. The fluid volume for this cubic closest packing example was 47.6 % of total volume. If NAPL in this space has a saturated thickness of 0.1 cm, then NAPL volume is calculated to be 2.15 cm^3 or 2.11 cc /liter. Using NAPL density, in this case diesel density of 0.832 g/l, concentration of NAPL in the pore space was 3.75 mg/l. If measured in a well, the

observed concentration of NAPL in the dissolved phase or the amount of NAPL thickness would depend on the capillary properties of the media and well construction (Marinelli and Durnford, 1996; Newell, 1995).

4.2 Tank Optical monitoring

Digital images collected during this experiment were used to produce saturation curves and to calculate mass concentrations for a specific time and location. These data were then used to create profiles to compare and integrate with the electrical resistivity data. From the point of NAPL introduction on the left end of the tank, the diesel infiltrated through the vadose zone until it reached the water table. Once diesel reached the water table, migration shifted to a lateral direction going from the left to the right side of the tank. The diesel plume thickness was greater at the left side, where the NAPL was introduced, and continued to thin out until it reached an end point at the right side, forming a wedge shape (Figure 5a). At the 10 cm lateral mark, for the first 6 days of experiment, the plume thickness ranged between 5.5 to 6.5 cm and gradually decreased with an increase in lateral distance.

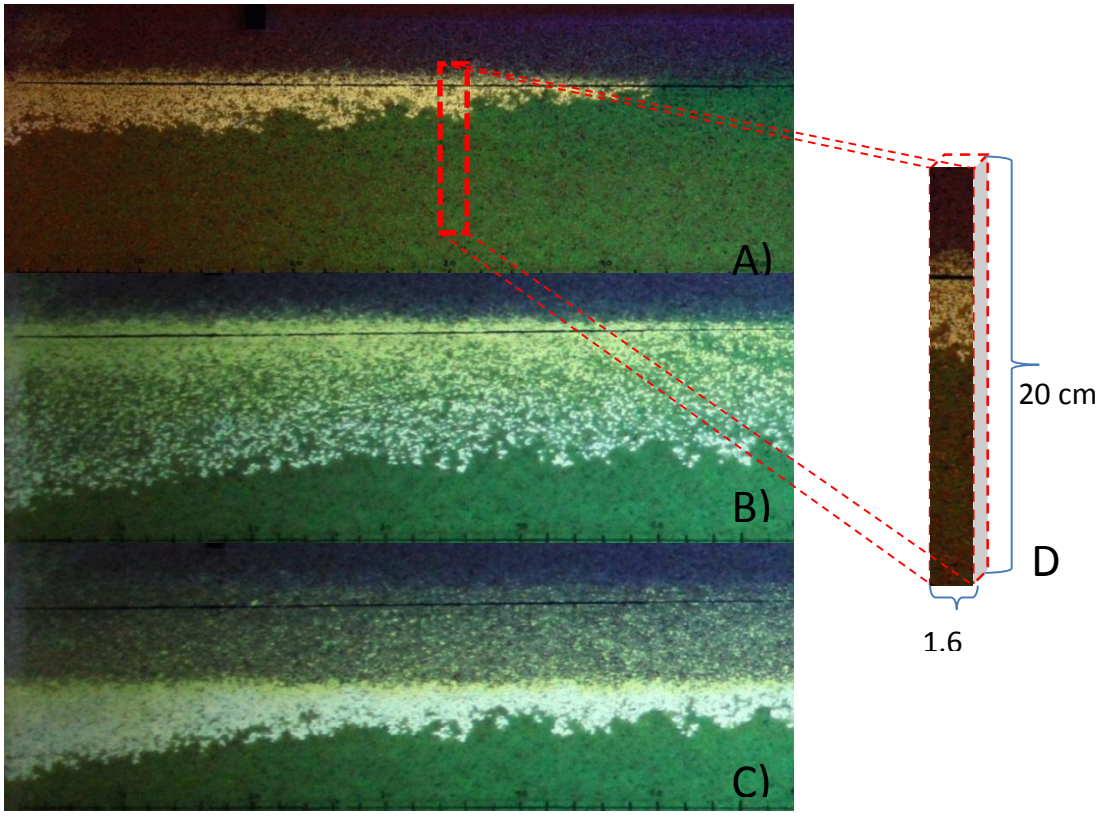

Figure 5. Digital images of diesel distribution: a) stable water table during first 6 days of

experiment (4th day) b) tidal stimulations when water table was lowest (14.29th day), c) tidal stimulations when water table was at original elevation (14.54th day) and d) An example of the element volume used to produce saturation curves.

The plume was first observed optically on the second day of the experiment. The plume had a length of 21 cm at this time, with a total of 3.8 g diesel introduced into the tank. The total length of the plume on the sixth day was 63 cm, with 277.4 g of diesel. Smearing simulations were performed for one day by changing the water table every 6 hours. The diesel smeared across the tank after the water table was lowered. Figure 5b shows the digital image taken at day 13.75, when the water level was highest (original level). Figure 5c shows the digital image taken at day 14.45when the water level was lowest (22 cm lower than original). During the smearing stimulation 642 g of diesel were in the tank and the plume length reached 170 cm. The plume thickness was approximately uniform across the tank, averaging around 12 to 14 cm in width. Smearing doubled the thickness of the plume from what had existed before changing the water level.

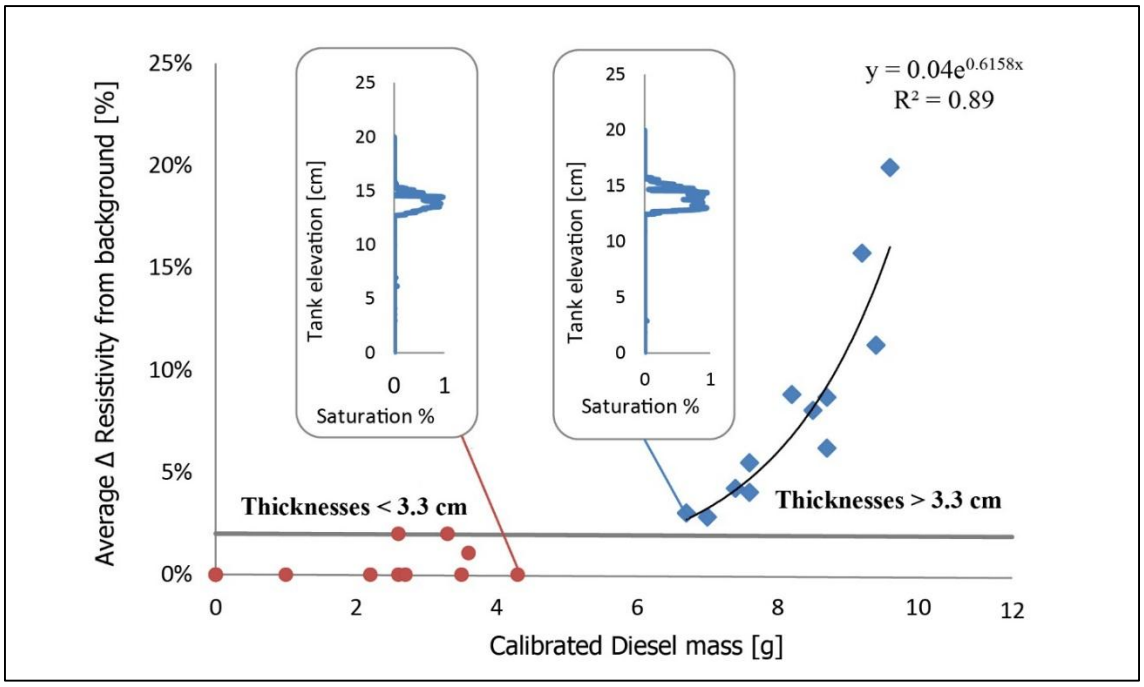

Figure 6. Correlation between thicknesses of impacted zone, diesel mass calibrated, and average change in resistivity for each element. The two inset graphs represent the

saturation profiles of two "element volumes" and the straight gray line denotes the resistivity background noise level of two percent.

In addition to optically monitoring the diesel migration, digital images were also used to calculate NAPL saturations. Two representative NAPL saturation curves generated from the digital images representing electrically undetected and electrically detected saturation curves indicate that the signal requires a full saturated portion of the plume to be detected (Figure 6). The first curve is a NAPL saturation profile extract from an "element volume" with a thickness smaller than 3.3 cm and a diesel mass of 4.3 [g]. The second saturation curve is extracted from an "element volume" with a thickness larger than 3.3 cm and a diesel mass of 6.7 [g]. A change in diesel mass corresponded to an increase in the diesel thickness and diesel saturation values although both profiles are similar in appearance (Figure 6).

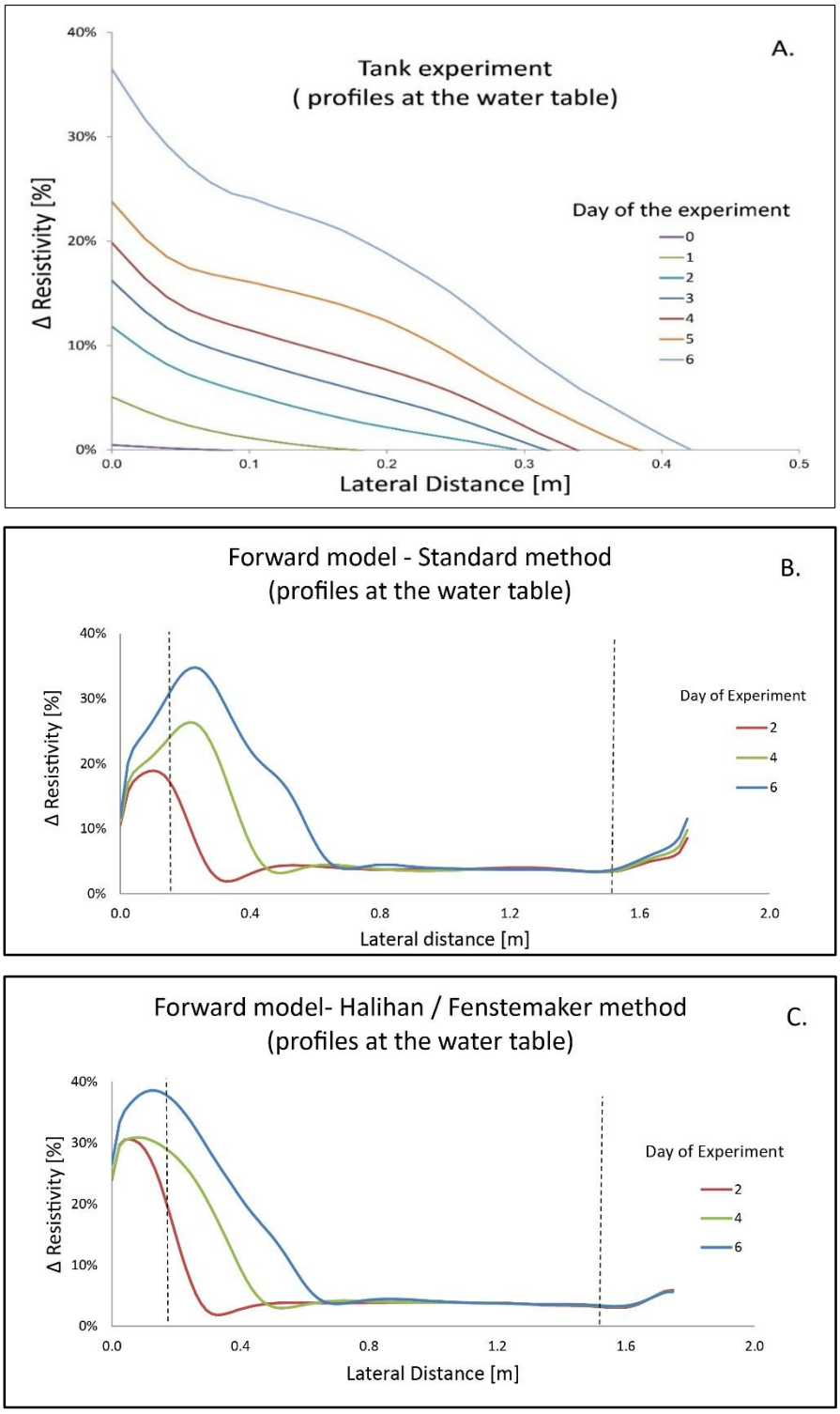

Figure 7. Horizontal resistivity differences at the water table during a specific day of the experiment: a) profiles from the tank experiment, b) model resistivity using standard method, c) model resistivity using Halihan / Fenstemaker method. The dashed lines represent the trapezoid boundaries created during ERI data processing.

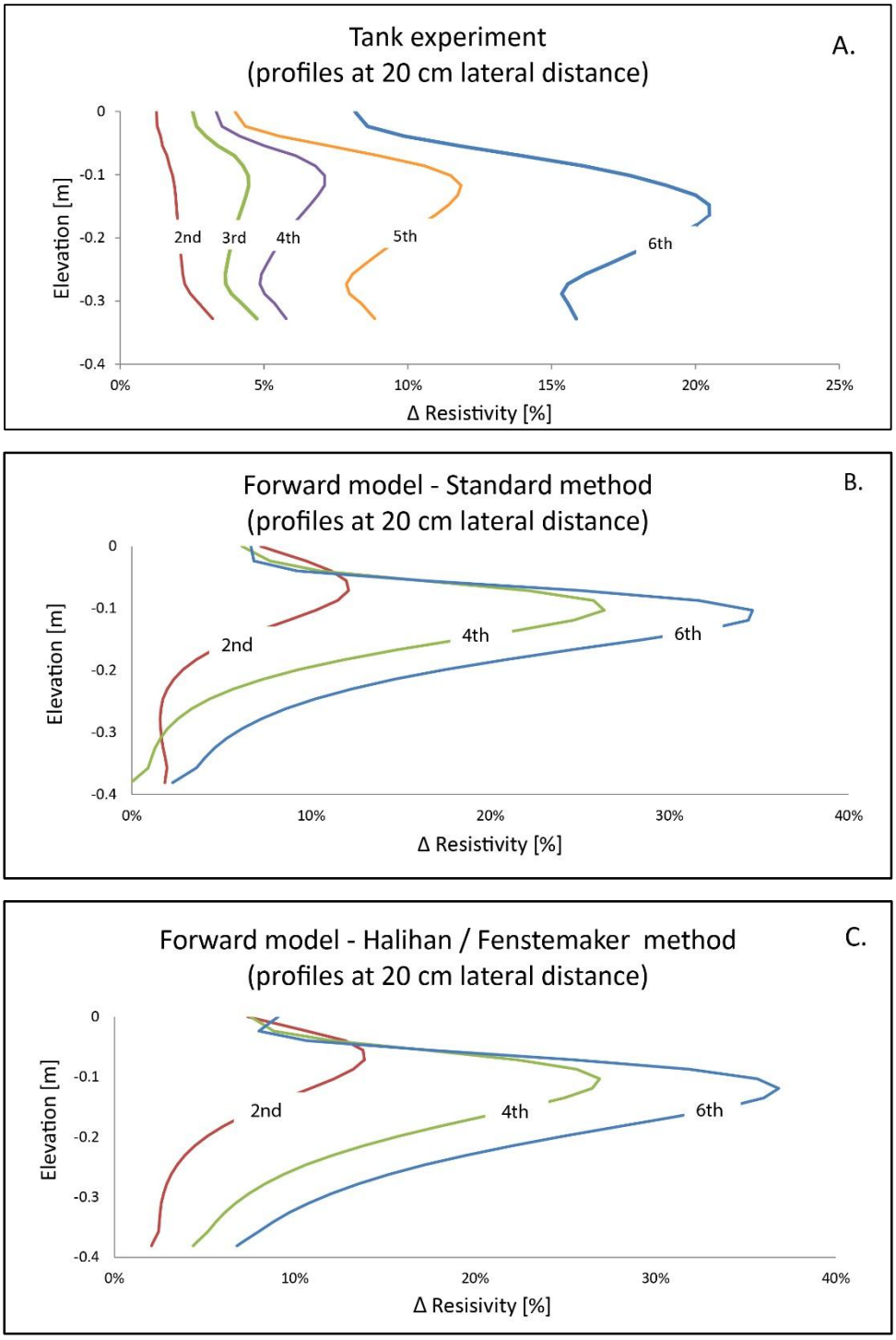

Figure 8. Vertical resistivity differences at 20 cm lateral distance during a specific day of the experiment: a) profiles from the tank experiment, b) model resistivity using standard method, c) model resistivity using Halihan / Fenstemaker method.

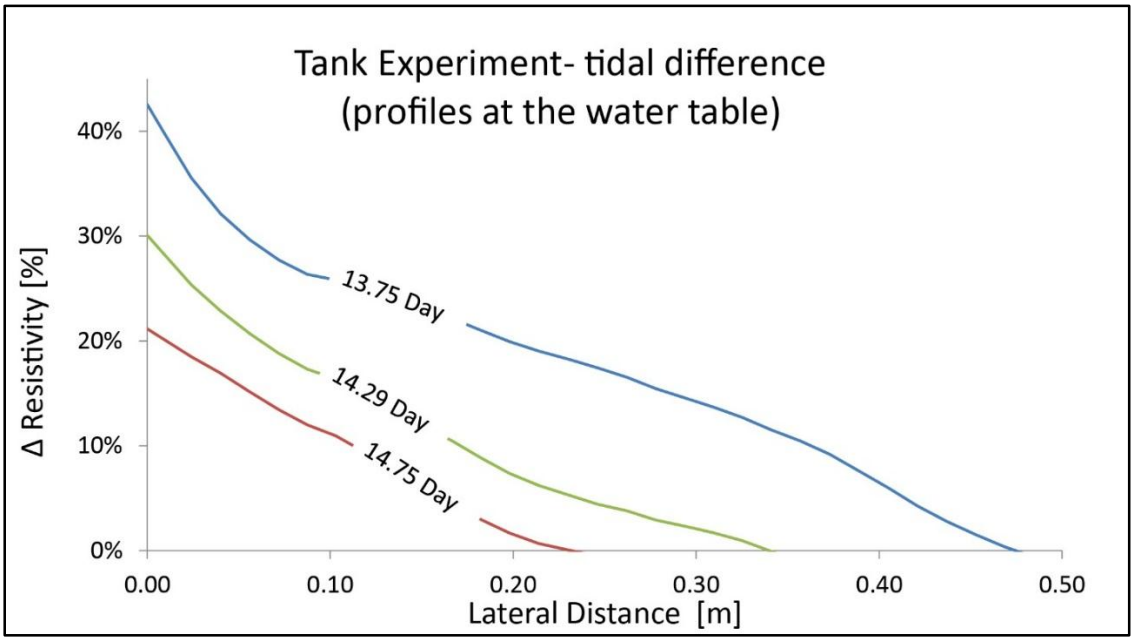

Figure 9. Tank resistivity differences at the water table for times during tidal stimulations. The data from 14.04 day and 14.54 day are not shown in the graph because of their change in resistivity higher than 300% which occurred when the water table was at low tide condition.

4.3 Tank Electrical monitoring

The data obtained from the sand tank experiment provide electrical resistivity profiles that reflect the NAPL migration observed optically. The results are shown using the Halihan/Fenstemaker methodology as the standard methodology could not obtain stable changes during the experiment. At the water table, the relative sensitivity of the Halihan/Fenstemaker methods was greater than two orders of magnitude above the standard methods. The resulting resistivity difference data show the NAPL front migrated laterally from the left side of the tank, where the spillage point occurred, towards the center of the tank (Figure 7a). As the experiment progressed in time, for a specific lateral distance, the change in resistivity increased from background for the monitoring of the plume migration across the tank. Additionally, change in resistivity decreased with an increase in lateral distance where the plume was thinner.

For the first two data sets collected prior to the generation of the NAPL plume, the maximum resistivity difference from background was approximately a change of 2 %.

This small change in resistivity was not a result of presence of NAPL in the tank, and was simply noise due to data collection and any changes in the electrode contact resistance due to evaporation or gel migration around the electrodes. With time, the plume length and thickness grew and as a result the maximum change in resistivity continued to increase. On the second day of the experiment (50^{th} hour) when the NAPL plume was present, the maximum change in resistivity was 11.8 %. Prior to tidal stimulation experiment on the sixth day, the peak change in resistivity 36.8 %.

On the second day of the experiment, the total plume length was 36 cm, however, only 25 cm of the plume were detected electrically, about 86% of the plume length. On the sixth day 61% of the plume was detected, out of a total plume length of 62 cm, 38 cm were detected electrically. On the other three days 70 % of the plume was detected, the plume ranged from 36 to 51.6 cm and 25 to 35 cm were detected respectively. In total, the electrical detection of the plume was 61%-86% of the total plume length. The remaining 11-20 cm that were not detected were the plume edge.

The vertical changes in resistivity for the first six days of the experiment, plotted at 20 cm lateral distance from the left edge of the tan, illustrate the resistivity difference from background increased with time (Figure 8). Peak anomalies were found very close to the water table, between 10 and 20 cm in depth. On the second day, changes in resistivity were minimal (below 5%) as a result of the plume length being only 21 cm long. The highest change in resistivity, a 22% increase at 20 cm laterally, was observed on the sixth day.

During smearing simulations, when the water table was high, equal to the original experimental level, changes in resistivity decreased over successive smearing cycles (Figure 9). As the experiment progressed with time, for the given lateral distance in meters, the resistivity difference from background decreased considerably. For example, for 10 cm lateral distances, the resistivity difference from background for days 13.75 and 14.75 were 26 % and 11 %, respectively. Water table profiles at days 14.04 and 14.54 are not shown in the graph because there are considerably higher changes in resistivity due to the unsaturated conditions in the area between the low water table and the original water table. Such profiles reached up to 300 % change in resistivity difference from background.

The relationship between calibrated diesel mass (independent variable) and average resistivity difference from background (dependent variable) for two plume thickness profiles is well correlated (Figure 6). The thicknesses of NAPL saturated zones were calculated from the saturation curves. The data were calculated per "element volume" (Figure 5d) at specific lateral distances (10, 20, 30, 40 and 50 cm and the edge of the plume) for the first six days of the experiment. Impacted zones with smaller than 3.3 cm diesel thickness, contained 0 to 4 grams of diesel in an elemental volume and an average resistivity difference between 0.0 and 2.0%. These profiles did not produce enough change in resistivity and were considered to be background variability. Profiles with thicknesses larger than 3.3 cm had approximately 7.0 to 9.6 grams of diesel and an average change in resistivity between 3.0% and 19.9%. Note that average change in resistivity increased dramatically for thicknesses larger than 3.3 cm.

4.4 Forward resistivity model results

A theoretical resistivity forward model simulating a single resistive layer, 1.5 cm thick, between a vadose and phreatic layer is used to illustrate a plume with uniform thickness across the tank. The resistivity forward models with a single resistive layer 30 cm long is used to simulate a plume of limited length (Figure 10).

The graph shows the extrapolated profile at the water table using Halihan / Fenstemaker methods, but similar profiles were generated using the standard method. For the model with uniform thickness across the tank Halihan / Fenstemaker method generated change in resistivity between 12 and 14 %. The black dashed lines represent the trapezoid boundaries that would be expected at the depth of the resistive layer in an inverted ERI dataset. As a result the resistivity difference values fluctuate on both edges of the model when they reach the model boundaries. From 0 to 0.18 m lateral distance the profiles experience a steep increase, then it levels out until it reaches 1.8 m lateral distance and the profiles start decreasing.

For the model with a single resistive layer 30 cm long, Halihan/ Fenstemaker method generated 13% change in resistivity, and at 18 cm lateral distance the signal starts decreasing and at 40 cm lateral distance it went down to 0% change. The model at 30 cm

lateral distance, where the plume edge is, had a change in resistivity of 6 %, demonstrating that theoretical models were able to detect the edge of the plume.

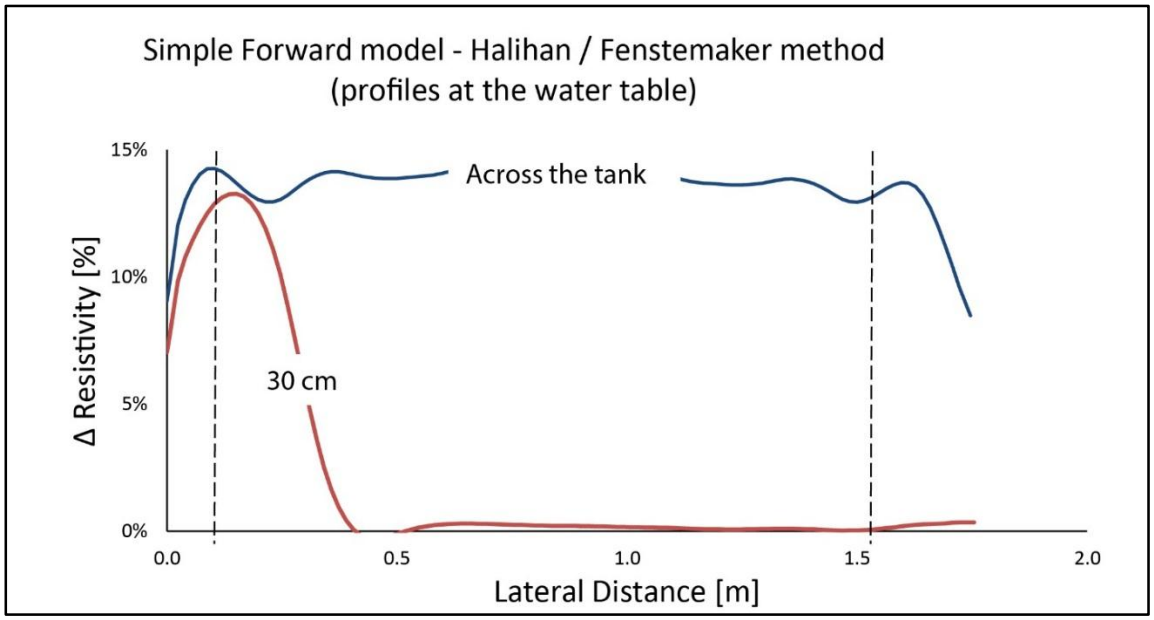

Figure 10. Simple forward model using Halihan / Fenstemaker method for two types of the resistive layer. The dashed lines represent the trapezoid boundaries created during ERI data processing.

Simple theoretical resistivity forward models with a resistive layer starting at 10 cm long and increasing by 10 cm where used to illustrate the impact of the length of the plume in the electrical signal (Figure 11) . The figure shows the data produced using the Halihan / Fenstemaker method, however, similar values were generated using the standard method. At 20 cm lateral distance change in resistivity values for 10 and 20 cm long resistive layer were less than 2 %, which was considered background. For 30 cm and longer resistive layer the model predicted a change in resistivity between 12 to 14%. Contrary to the tank experiment the change in resistivity did not increase with increase of the plume length as the model thickness was constant.

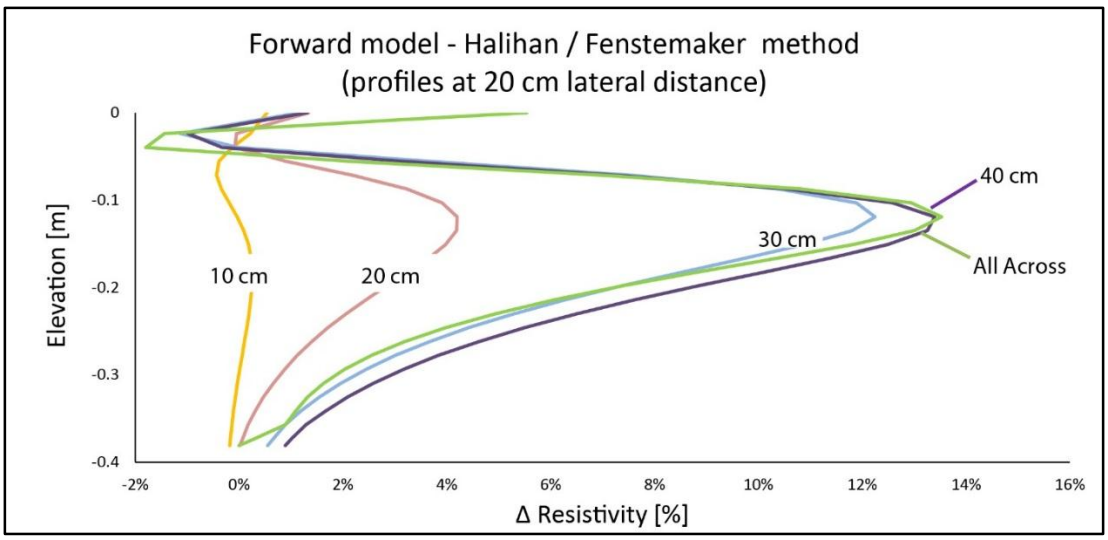

Figure 11. Change in resistivity at 20 cm lateral distance for a simple forward model with varying plume lengths.

The results of the simple theoretical resistive model evaluating changes in the background resistivity illustrate strong increase in resistivity changes as the background resistivity becomes more conductive (Figure 12). The results on the graph are the results generated using the Halihan/ Fenstemaker method, but similar values were produced using the standard method. At 20 cm lateral distance for background resistivity decreasing from 800 to 200 [Ohm–m], the change in resistivity increased from 15 to 85%.

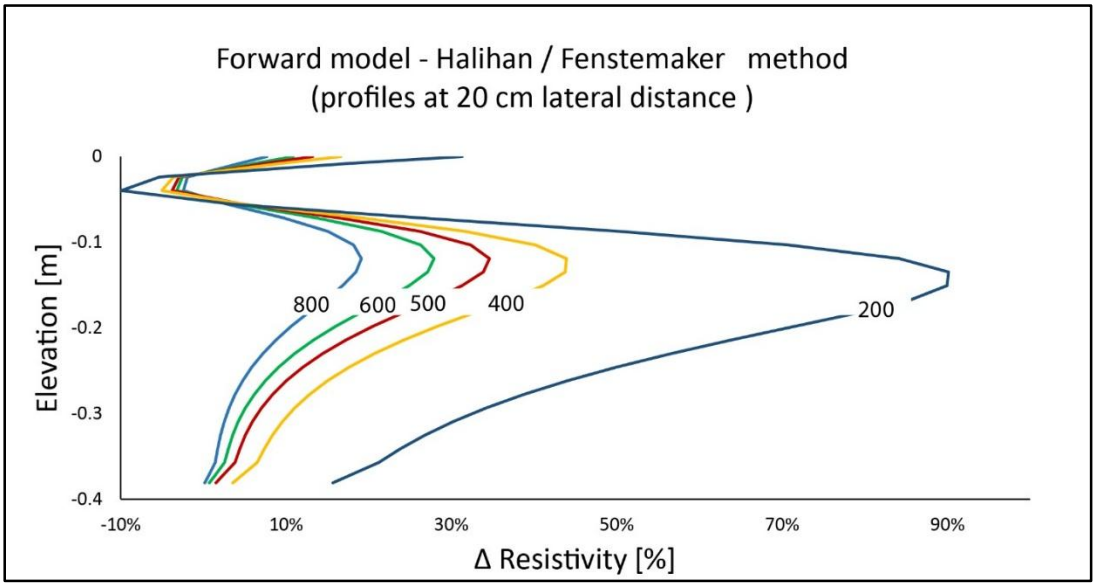

Figure 12. Change in resistivity for a simple forward model when the background resistivity [Ohm-m] was reduced relative to the saturated NAPL layer.

Forward resistivity models that replicate the plume thickness and length from the tank experiment, were conducted to compare and assess the electrical signal between the tank experiment and the models (Figure 7 b & c). For a specific lateral distance both the standard and the Halihan / Fenstemaker method show that resistivity difference increased with time. As an example, at 20 cm lateral distance resistivity difference for the standard method, for the second and the sixth day, was 13% and 34%, respectively. For the same given lateral distance and specific days, the resistivity difference using Halihan / Fenstemaker method was 28% and 35%, respectively.

Both methods detected the "plume edge" in all three days in the model simulations. The standard method's resistivity difference peaked at 22 cm lateral distance, whereas the Halihan / Fenstemaker method peaks were shifted to 18 cm lateral distance mark. The standard method profiles had a sharp decrease of resistivity difference with lateral distance, while the Halihan / Fenstemaker method profiles had a smoother decrease.

The resistivity difference profiles for both methods show the increase in resistivity difference as the model plume size increased (Figure 8 b & c). Additionally, both methods had anomalies located very close to the water table between 7 and 15 cm depth. The standard method has a slightly smaller resistivity difference than the Halihan / Fenstemaker method. The maximum resistivity difference for the second and sixth day using the standard method were 12% and 35 %, while, for the Halihan / Fenstemaker method were 14% and 38 %, respectively.

CHAPTER V

DISCUSSION

This research was conducted to evaluate the mechanism for detecting small quantities of non- aqueous phase liquids in subsurface environments with electrical resistivity. To test the hypothesis that the NAPL creates a barrier that impacts the current flow and increase the bulk resistivity of the media three different approaches were taken. These three approaches as well as future work that could improve this research are discussed below.

5.1 NAPL restive barrier mechanism

The hypothesis was supported by the theoretical model. The theoretical model illustrates how a NAPL creates a barrier that affects the electrical current, creating an insulating layer which leads to the high resistivity signal generated at fresh water environmental sites without requiring a significant mass (Figure 1). This explains that the mechanism for detecting NAPL electrically is directly related to the geometric distribution of the fluid phase NAPL, and not the bulk quantity in the pore space. It is important to say that from the known NAPL thickness at a specific location it is possible to mathematically calculate the NAPL concentration in non-aqueous and dissolved phases, but difficult to estimate the amount of free phase NAPL that would be observed in a monitoring well due to capillary effects (Newell, 1995).

5.2 Laboratory tank experiment (optical and electrical monitoring)

The sand tank used for this experiment was constructed from glass walls within a metal frame and optimized for optical monitoring experiments. To enhance the visualization of the NAPL florescent dyes and UV light were employed in a matrix of clean white sand.

The saturation data retrieved from this technique calculated the saturation for a 2D image, however, assuming a uniform porosity throughout the tank, as well as uniform saturation through the width of the tank for a particular location in our case for the "element volume", allowed us to calculate the NAPL mass for a specific volume space. The saturation data were sensitive to the image results (Figure 9). For example, a saturation value of 0 % was located in the in the middle of the impacted zone as a result of the black line marked in centimeters on front of the tank for distance and water table elevation. The MATLAB® program, because of the black color, assumed that the area where the line was located was not saturated with NAPL, where in fact the line was located right in the middle of the impacted zone. This did not significantly affect the results, but affects how the front of the tank is labeled for scale.

As time progressed, the amount of diesel spilled in the tank increased, resulting in a thicker and longer plume as well as higher diesel saturation levels. A larger NAPL thickness produced a greater resistive anomaly, indicating that the electrical resistive signal is highly affected by the thickness of the saturated impacted zone. In this experiment ERI was able to detect thicknesses greater than 3.3 cm with only 7 g of diesel in the "element volume". As the plume length increased, the NAPL saturation decreased resulting in very thin edges (less than 3.3 cm) with low NAPL saturations. As a result of the plume thinning with increasing length, the total plume length detection decreased from 80% on the second day to 60% on the sixth day of the experiment.

Smearing simulations were also performed to demonstrate the effects of bulk fluid free phase NAPL on the electrical signal**.** The results show that water table oscillations decreased the electrical signal detected. This was directly linked to diesel migrating vertically during the changes in water table elevation. This migration distributed the diesel concentration throughout the tank creating a smear zone of lower saturations. Conversely, at the times when the water table was low the resistivity changes were high, with up to 300% resistivity difference from background as a result of the pores being filled with air creating a more resistive media. The water table oscillation experiment also supports the theory that the electrical signal generated is a result of the free NAPL that is concentrated in a layer creating a blocking / barrier layer.

5.3 Forward resistivity models

Two sets of forward models were used to compliment the data from the tank experiment. The first set was a simple theoretical forward model with a single resistive layer going across the tank and the second set replicated the plume thicknesses and length from the tank experiment. The models predicted a resistive layer "plume" that is 100 % saturated with no lateral or vertical shifts, just a sharp boundary, which differs from the tank experiment where NAPL saturations decreased with increase in lateral distance and were distributed vertically. Because of this assumption the electrical signal generated in the forward models differed from the tank experiment. Higher changes in resistivity were generated from the models, and the models detected the exact edge of the plume. However, the general trend of the profiles generated were similar from both the forward models and the tank experiment. The profiles generated from the simple models had obvious boundary effects on both side of the tank. During data processing the inversion resistivity section creates a trapezoid shape leaving out some of the data in the edges. Forward model profiles also demonstrate that the thickness of the layer, in our case NAPL "plume", has a direct effect on the electrical signal. Thicker resistive layers generated a larger electrical signal as a change in resistivity. Furthermore, the forward model illustrated that at a particular lateral distance the electrical signal is not impacted by the length of the plume, for example at 20 cm lateral distance the change in resistivity values were similar for all the model plumes 30 cm and longer.

Models which altered the background resistivity indicated that decreasing the background resistivity, making the media more conductive, the electrical signal generated from the resistive layer is much larger. This effect likely contributed to the success of field experiments performed prior to this work in more conductive settings (Halihan et al., 2005). This increase in signal is not simply due to the more conductive background resistivity, but the change in the ratio between the two resistivities (native and impacted zones). This suggested that DNAPLs should provide a stronger resistivity signature than LNAPLs as they are more electrically resistive materials. This is supported by the signatures observed on DNAPL field sites (Halihan et al., 2012).

Additionally, the model resistivity varied relative to the tank resistivity inversions at the boundaries of the images. While both model and tank resistivity differences were

calculated using the same assumptions, the tank varied from these assumptions and the field setting of previous experiments. The tank boundary was a resistive boundary acting as a no flow boundary where the models are assuming an infinitely wide half space. This is the source of differences in the edges of the models compared with the tank data (Figures 6 and 9). Experimental plumes in the center of the domain would allow this effect to be eliminated from future experiments as half space modeling is useful for comparison to field settings.

5.4 Future work

These types of experiments can be improved to determine additional information on the migration and detection of NAPLs in the subsurface. Due to the conductivity of the metal frame, this tank was not optimal for resistivity monitoring. The tank was sealed for water leakage, yet small quantities of water were observed coming out from the edges where the glass walls and metal frame were joined. These possible connections between tank fluid and the metal frame added noise to the ERI data on the edges of the tank. This issue did not have a significant effect on the ERI data collected in the shallow portion of the tank, where most of the diesel was located. In future experiments, nonmetallic tank setups would be optimal.

One of the problems that can be approached differently in this experiment is to change the location of diesel additional location. Instead of introducing the diesel on the left corner of the tank, which forces the diesel to migrate to the right side of the tank, one option is to introduce the diesel in the center of the tank. This would generate an equal diesel distribution in both sides and it would eliminate boundary conditions in the ERI datasets at the edges of the tank.

This experiment used a clean white sand as it provided a good contrast for the optical experiments, but was highly resistive, adding a source of noise to the experiment due to difficulties electrically coupling the electrodes to the tank surface. An experiment with a conductive media might be a better example of field conditions and crucial to understand the mechanism and appropriately quantify the resistivity values. This would improve the electrical data in the experiment, but would likely come at a degradation of high quality optical saturation data.

Ultimately, future research could experiment with a tank with biodegraded diesel fuel or with bioremedies added to the tank. Previous studies have demonstrated that a conductive geophysical signal can be generated in the area were NAPL is present (Atekwana et al., 2000). The diesel used in this research was fresh and generated a resistive geophysical signal. Using old, biodegraded diesel or one that undergoes biodegradation might be beneficial to better understand effectiveness of the mechanism that generates conductive geophysical signals. These experiments have been conducted in columns (Cassidy et al., 2001) but understanding the two dimensional growth patterns and how they look in electrical data would be useful for field interpretation.

CHAPTER VI

CONCLUSION

Detectable increases in electrical resistivity can be generated by small part per million quantities of NAPL in porous media. The mechanism for generating this signal is free phase NAPL in pore throats blocking the flow of electrical current. A sand tank was utilized to optically and electrically monitor the migration of NAPL, and together with a theoretical model and forward resistivity models, the data supported the hypothesis that ERI can detect small quantities of NAPL in subsurface environments and that the free phase NAPL on top of the water table creates an electrical barrier that is the primary source of the resistive electrical signal generated. The results of this research supported the theory that NAPL can be detected at low bulk concentrations and the amount of the resistive geophysical signal generated is directly affected by the saturated thickness of the impacted zone. In the tank experiment, a larger resistivity difference was generated as the plume became the thicker and more saturated when the plume thickness was greater than 3.3 cm. However, as the time progressed the plume got longer and thinner with low NAPL saturated thickness at the edges, affecting the percentage of the plume length detection, ranging from 61-86% of the total plume length.

The experiment also used water table oscillations to monitor the effects bulk fluid concentration had on the geophysical signal. Once the water table was cycled, the NAPL smeared across the tank causing the electric resistivity differences to decrease. The mechanism suggests that the geometric distribution of phase separated hydrocarbons control the NAPL detection electrically over the bulk concentration of hydrocarbons.

This tank experiment was conducted in extremely resistive conditions, resulting in a small electrical signal. However, if this experiment was to be undertaken in a more electrically conductive matrix, more common in the subsurface environment, forward modeling suggests that the geophysical signal generated as a result of NAPL would be greater.

REFERENCES

Adepelumi, A., Solanke, A., Sanusi, O., and Shallangwa, A., 2006, Model tank electrical resistivity characterization of LNAPL migration in a clayey-sand formation: Environmental geology, v. 50, no. 8, p. 1221-1233.

Apparao, A., Roy, A., and Mallick, K., 1969, Resistivity model experiments: Geoexploration, v. 7, no. 1, p. 45-54.

Atekwana, E. A., Sauck, W. A., and Werkema Jr, D. D., 2000, Investigations of geoelectrical signatures at a hydrocarbon contaminated site: Journal of Applied Geophysics, v. 44, no. 2–3, p. 167-180.

Benson, A. K., and Mustoe, N. B., 1998, Integration of electrical resistivity, ground-penetrating radar, and very low-frequency electromagnetic induction surveys to help map groundwater contamination produced by hydrocarbons leaking from underground storage tanks: Environmental Geosciences, v. 5, no. 2, p. 61-67.

Benson, A. K., Payne, K. L., and Stubben, M. A., 1997, Mapping groundwater contamination using DC resistivity and VLF geophysical methods-A case study: Geophysics, v. 62, no. 1, p. 80-86.

Bentley, L. R., and Gharibi, M., 2004, Two-and three-dimensional electrical resistivity imaging at a heterogeneous remediation site: Geophysics, v. 69, no. 3, p. 674-680.

Blunt, M. J., 2001, Flow in porous media — pore-network models and multiphase flow: Current Opinion in Colloid & Interface Science, v. 6, no. 3, p. 197-207.

Brewster, M., Annan, A., Greenhouse, J., Kueper, B., Olhoeft, G., Redman, J., and Sander, K., 1995, Observed migration of a controlled DNAPL release by geophysical methods: Groundwater, v. 33, no. 6, p. 977-987.

Burger, H. R., Sheehan, A. F., and Jones, C. H., 2006, Introduction to applied geophysics: Exploring the shallow subsurface, WW Norton.

Cassidy, D. P., Werkema Jr, D. D., Sauck, W., Atekwana, E., Rossbach, S., and Duris, J., 2001, The effects of LNAPL biodegradation products on electrical conductivity measurements: Journal of Environmental & Engineering Geophysics, v. 6, no. 1, p. 47-52.

Chambers, J., Loke, M., Ogilvy, R., and Meldrum, P., 2004, Noninvasive monitoring of DNAPL migration through a saturated porous medium using electrical impedance tomography: Journal of contaminant hydrology, v. 68, no. 1, p. 1-22.

Chambers, J., Wilkinson, P., Wealthall, G., Loke, M., Dearden, R., Wilson, R., Allen, D., and Ogilvy, R., 2010, Hydrogeophysical imaging of deposit heterogeneity and groundwater chemistry changes during DNAPL source zone bioremediation: Journal of contaminant hydrology, v. 118, no. 1, p. 43-61.

Chapman, S. W., Parker, B. L., Sale, T. C., and Doner, L. A., 2012, Testing high resolution numerical models for analysis of contaminant storage and release from low permeability zones: Journal of contaminant hydrology, v. 136, p. 106-116.

Cook, K. L., and Van Nostrand, R. G., 1954, Interpretation of resistivity data over filled sinks: Geophysics, v. 19, no. 4, p. 761-790.

Daily, W., Ramirez, A., Binley, A., and LeBrecque, D., 2004, Electrical resistance tomography: The Leading Edge, v. 23, no. 5, p. 438-442.

Daniels, J. J., Roberts, R., and Vendl, M., Site studies of ground penetrating radar for monitoring petroleum product contaminants, *in* Proceedings Proceedings of the Symposium on the Application of Geophysics to Engineering and Environmental Problems1992, Volume 2, The Society, p. 597.

Dawalibi, F., and Mukhedkar, D., 1974, Ground electrode resistance measurements in non uniform soils: Power Apparatus and Systems, IEEE Transactions on, no. 1, p. 109-115.

Delaney, A. J., Peapples, P. R., and Arcone, S. A., 2001, Electrical resistivity of frozen and petroleum-contaminated fine-grained soil: Cold Regions Science and Technology, v. 32, no. 2–3, p. 107-119.

DeRyck, S., Redman, J., and Annan, A., Geophysical monitoring of a controlled kerosene spill, *in* Proceedings Proceedings of the Symposium on the Application of Geophysics to Engineering and Environmental Problems (SAGEEP'93), San Diego, CA1993, p. 5-20.

Endres, A. L., and Redman, J. D., 1996, Modelling the electrical properties of porous rocks and soils containing immiscible contaminants: Journal of Environmental and Engineering Geophysics, v. 1, no. B, p. 105-112.

Halihan, T., Paxton, S., Graham, I., Fenstemaker, T., and Riley, M., 2005, Post-remediation evaluation of a LNAPL site using electrical resistivity imaging: Journal of Environmental Monitoring, v. 7, no. 4, p. 283-287.

Hawkins, A. M., 2013, Processes controlling the behavior of LNAPLs at groundwater surface water interfaces: Colorado State University.

Hofstee, C., Oostrom, M., Dane, J., and Walker, R., 1998, Infiltration and redistribution of perchloroethylene in partially saturated, stratified porous media: Journal of contaminant hydrology, v. 34, no. 4, p. 293-313.

Hosseini, S., Patel, D., Ein-Mozaffari, F., and Mehrvar, M., 2010, Study of solid–liquid mixing in agitated tanks through electrical resistance tomography: Chemical Engineering Science, v. 65, no. 4, p. 1374-1384.

Kamon, M., Endo, K., Kawabata, J., Inui, T., and Katsumi, T., 2004, Two-dimensional DNAPL migration affected by groundwater flow in unconfined aquifer: Journal of Hazardous Materials, v. 110, no. 1–3, p. 1-12.

Kostarelos, K., Pope, G. A., Rouse, B. A., and Shook, G. M., 1998, A new concept: the use of neutrally-buoyant microemulsions for DNAPL remediation: Journal of Contaminant Hydrology, v. 34, no. 4, p. 383-397.

Loke, M., 2000, Electrical imaging surveys for environmental and engineering studies.

Marinelli, F., and Durnford, D. S., 1996, LNAPL thickness in monitoring wells considering hysteresis and entrapment: Groundwater, v. 34, no. 3, p. 405-414.

Monier-Williams, M., Properties of light non-aqueous phase liquids and detection using commonly applied shallow sensing geophysical techniques, *in* Proceedings Proceedings of the Symposium on the Application of Geophysics to Engineering and Environmental Problems (SAGEEP'95), Orlando, FL1995, p. 1-13.

Neumann, T. C., Valsangkar, A. J., and MacQuarrie, K. T. B., 2000, Physical Modelling Of Lnapl Infiltration In A Variably-Saturated Sand, International Society for Rock Mechanics.

Newell, C. J., 1995, Light nonaqueous phase liquids, United States Environmental Protection Agency, Office of Research and Development, Office of Solid Waste and Emergency Response: Superfund Technology Support Center for Ground Water, Robert S. Kerr Environmental Research Laboratory.

Nyquist, J. E., Freyer, P. A., and Toran, L., 2008, Stream Bottom Resistivity Tomography to Map Ground Water Discharge: Ground Water, v. 46, no. 4, p. 561-569.

Oostrom, M., Hofstee, C., Walker, R. C., and Dane, J. H., 1999, Movement and remediation of trichloroethylene in a saturated heterogeneous porous medium: 1. Spill behavior and initial dissolution: Journal of Contaminant Hydrology, v. 37, no. 1–2, p. 159-178.

Reynolds, J. M., 2011, An introduction to applied and environmental geophysics, John Wiley & Sons.

Sale, T., Taylor, G. R., Iltis, G., and Lyverse, M., 2007, Measurement of LNAPL Flow Using Single-Well Tracer Dilution Techniques: Groundwater, v. 45, no. 5, p. 569-578.

Schneider, G. W., and Greenhouse, J. P., Geophysical detection of perchloroethylene in a sandy aquifer using resistivity and nuclear logging techniques, *in* Proceedings Proceedings of the Symposium on the Application of Geophysics to Engineering and Environmental Problems1992, Volume 2, The Society, p. 619.

Singh, J., Jha, B. P., and Gupta, R. P., 1971, Model tank experiments for resistivity measurements on non-conducting and conducting sheets: pure and applied geophysics, v. 85, no. 1, p. 90-106.

Slater, L., Binley, A., Versteeg, R., Cassiani, G., Birken, R., and Sandberg, S., 2002, A 3D ERT study of solute transport in a large experimental tank: Journal of Applied Geophysics, v. 49, no. 4, p. 211-229.

Smith, R. C., and Sjogren, D. B., 2006, An evaluation of electrical resistivity imaging (ERI) in Quaternary sediments, southern Alberta, Canada: Geosphere, v. 2, no. 6, p. 287-298.
Telford, W. M., Sheriff, R. E., and Geldart, L. P., 1990, Applied geophysics, Cambridge university press.
Van Geel, P. J., and Sykes, J. F., 1994, Laboratory and model simulations of a LNAPL spill in a variably-saturated sand, 1. Laboratory experiment and image analysis techniques: Journal of Contaminant Hydrology, v. 17, no. 1, p. 1-25.
Yang, C. H., Yu, C. Y., and Su, S. W., 2007, High resistivities associated with a newly formed LNAPL plume imaged by geoelectric techniques - a case study: Journal of the Chinese Institute of Engineers, v. 30, no. 1, p. 53-62.

VITA

Valina Sefa

Candidate for the Degree of

Master of Science

Thesis: MECHANISM FOR DETECTING NAPL IN GROUNDWATER WITH RESISTIVITY

Major Field: Environmental Science

Biographical:

Education:

Completed the requirements for the Master of Science in Environmental Science at Oklahoma State University, Stillwater, Oklahoma in, July, 2015.

Completed the requirements for the Bachelors of Science in Environmental health and Science in your major at East Central University, Ada, Oklahoma in, May, 2012

Experience:
2012 – 2014 Research Assistant for an RMP project for Oklahoma State Parks

Professional Memberships:
Graduate and Professional Student Government
Society of Environmental Science